

LOCAL AIR QUALITY AND NOISE OPTIMIZATION OF A LARGE ASPECT RATIO WINGS WITH DISTRIBUTED HYBRID ELECTRIC PROPULSION

R. Cavallaro¹, Pablo Norczyk Simon¹ & Andrea Cini¹

¹Universidad Carlos III de Madrid, Avenida Universidad 30, 28911 Leganés, Spain. Corresponding Author: rauno.cavallaro@uc3m.es

Abstract

Achieving climate neutrality in aviation necessitates the development of innovative technologies and operational strategies. The INDIGO project, funded under the Horizon Europe programme, introduces a novel midrange aircraft featuring distributed hybrid electric propulsion (DHEP) and Large Aspect-Ratio Wings (LARW). To accurately evaluate trade-off solutions, a multidisciplinary optimization framework was developed. This framework incorporates advanced design and simulation tools to balance aerodynamic performance, fuel efficiency, and emissions reduction. The introduction of LARW-DHEP shows potential for significant emissions reductions, particularly during climb and landing operations. The INDIGO project approach highlights the feasibility and benefits of integrating DHEP and LARW in future aircraft designs, demonstrating the importance of holistic optimization in achieving sustainable aviation goals.

Keywords: LAQN; hybrid-electric aircraft; MDO; Strut-braced wings; OpenMDAO

1. Introduction

The aviation industry is currently facing a critical transformation, driven largely by the pressing need to cut down greenhouse gas emissions. The aim is to achieve a 33% emission decrease by the year 2030 and realize climate neutrality by 2050, in line with the goals set forth in the 2015 Paris Agreement [1]. This represents an extremely challenging task, especially considering aviation contribution of about 5% to the global warming issue, primarily through CO2 emissions from kerosene fueled aircraft[2]. In an effort to minimize its environmental impact, the sector is actively pursuing and investing alternative propulsion technologies.

One of the most promising technologies towards CO2 emissions reduction is hybrid-electric systems, which have shown the potential emission reductions compared to standard aviation fuels. These systems, which merge traditional gas turbines with electric power trains, offer a blend of efficiency and flexibility [3, 4]. They are capable of powering a diverse array of aircraft models and sizes, making them suitable for a wide range of flight missions. This versatility gives them an edge over purely battery-driven electric propulsion, allowing for a smoother transition into electrification while adapting to the evolving battery technologies .

A novel technology that is promising and leverages the efficiency and flexibility provided by placing small electric power units and propellers is Distributed Electric Propulsion (DEP) [5, 6]. Such systems leverage advancements in powerful, lightweight electric motor technologies, facilitating the spread of propulsive power among numerous propellers. The configuration not only allows aircraft to take off over shorter distances due to enhanced lift but could also contribute to a reduction in noise footprint by distributing power across several smaller electric-motor-driven propellers with lower tip mach numbers, leading to a reduction of the acoustic impact.

Another novel technology is the Large Aspect Ratio Wings (LARW) which increases aerodynamic efficiency by minimizing induced drag, which, in turn, boosts fuel efficiency. The synergistic integration

of the two technologies leads to the Large Aspect-Ratio Wings Distributed Hybrid Electric Propulsion (LARW-DHEP) system. This novel aircraft introduces a complex array of choices and trade-offs for engineers to consider. This intricacy, combined with the limited historical data on these advanced designs, underscores the importance of sophisticated sizing tools for preliminary feasibility studies Notably, tools based on Multi-Disciplinary Analysis and Optimization (MDAO) [7, 8] are incredibly useful. MDAO treats the design process of aircraft architectures as a problem of numerical optimization, facilitating a thorough comparison of different design pathways. By integrating analyses from various disciplines into a cohesive framework, MDAO allows for the simultaneous optimization of aircraft designs across multiple criteria, ensuring a balanced and effective design process. This not only speeds up the development of viable and groundbreaking aircraft designs but also enhances the capacity to investigate and assess novel solutions in a way that sequential optimizations cannot.

The foremost goal of this study is to create numerical models aimed at enhancing the design of a LARW-DHEP regional aircraft. This design mirrors the specifications of a model comparable to an Airbus A320 in terms of maximum payload. However, it is tailored for a mission of 1000 nautical miles at maximum payload.

The study focuses on the sizing of powertrain components and propellers, and examining the structural implications of novel technologies like hybrid-electric power systems and expanded wingspan into the aircraft design. The optimization process leverages the MDAO for Sustainable Aviation (MOTIVATION) framework, born a as fork from an OpenConcept [9], and initially conceived for enhancing hybrid-electric turboprops and subsequently extended to include also H2-burning turbofans [10]. The MOTIVATION framework has undergone further refinement for the INDIGO project [11] to incorporate innovative blowing and noise control technologies developed by project collaborators alongside a novel parallel-serial hybrid configuration.

1.1 The INDIGO project

The INDIGO project (Integration and Digital Demonstration of Low-emission Aircraft Technologies and Airport Operations), financed within the Horizon Europe programme, reunites academia, research centres and airports to identify the margins of improvement in airport Local Air Quality and Noise (LAQN) resulting from the introduction of a new non-conventional mid-range aircraft. The novel airframe features distributed propulsion based on hybrid electric/sustainable and conventional fuel powertrain and large aspect-ratio wing capable to fly quietly and in zero-to-low-emission mode (i.e. electric and SAF) at low altitudes near airports and resorts to conventional aviation fuel only when required, e.g., at higher altitudes or to recharge batteries during cruise. The novelty in each of these three dimensions (powertrain, airframe, operations) calls for an approach integrating all these aspects in the early design phases. Likewise, each technology needs a reliable performance prediction approach as previous industrial experience is not available.

One of the first technical deliverables of the project is a preliminary concept of the LARW-DHEP aircraft. Such preliminary aircraft will serve as a first basis for assessing the LAQN indices considering current and future air traffic scenario on European airports. This paper focuses on the design of such a preliminary version of LARW-DHEP aircraft.

The INDIGO consortium is led by Universidad Carlos III de Madrid (UC3M), and partners are *Centro Italiano Ricerche Aerospaziali SCPA* (CIRA), *Ruhr-Universitaet Bochum* (RUB), *Technische Universitaet Braunschweig* (TUB), *Barcelona Supercomputing Center Centro Nacional De Supercomputacion* (BSCN), *Deutsches Zentrum Fur Luft - Und Raumfahrt Ev* (DLR), *Centro De Referencia Investigacion Desarrollo E Innovacion Atm* (CRIDA), *Starptautiska Lidosta Riga Airport* (RIGA), *University Of Bristol* (UoB) and *University Of Strathclyde* (UoS).

1.2 Paper structure

The paper structure unfolds as follows: first, the various implemented modules are explained, then the optimization campaign is detailed, followed by the results from a case study and concluding with an explanation of the current state of work.

2. Methodology

The preliminary optimization carried out within the INDIGO framework is developed using MOTIVA-TION. MOTIVATION is a Python-written tool built on top of OpenMDAO[12], an open-source library for the development of multidisciplinary optimization problems. In OpenMDAO, MOTIVATION is linked

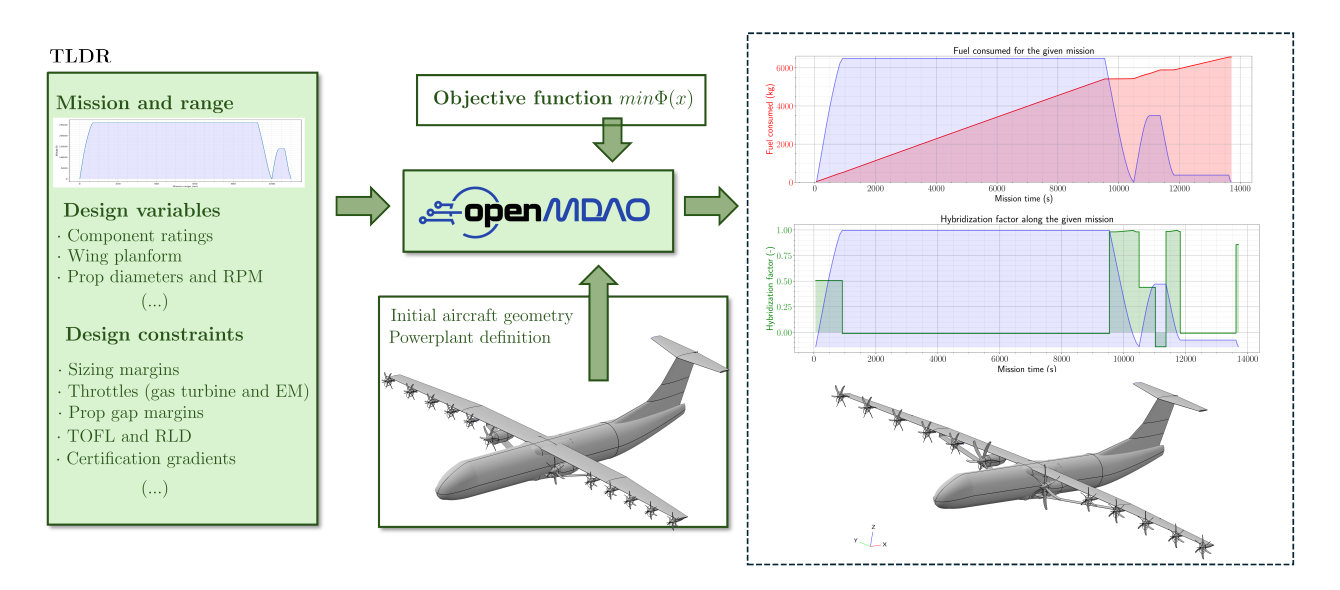


Figure 1 – Description of the MDAO optimization process.

to the problem by defining inputs such as mission specifications, chosen powertrain architecture, and baseline aircraft data, along with design variables like propeller diameter and component rating values. Constraints, such as maximum takeoff length and propeller gap margins, as well as objectives like minimizing emissions and noise during takeoff, are specified. Using this information, the framework then carries out simulations for the aircraft based on a specified FAR25-certified mission and optimizes the design variables to achieve the objective while adhering to the given constraints. A simplified version of this process is illustrated in Fig.1. It should be noted that there are no current certification specifications for novel aircraft configurations such as the one studied in INDIGO; however, inspiration is taken from FAR25 in terms of minimal performances, as it will be apparent in the next sections.

2.1 Baseline definition

The reference aircraft selected for this project is the A320, which has a Maximum Payload Weight (MPW) of 20 tons and a Maximum Takeoff Weight (MTOW) of 79 tons. INDIGO baseline, while aiming to maintain the same MTOW and MPW, is optimized for a nominal mission range of 1000 NM (with MPW), making it ideal for covering Europe most commonly operated routes. The wing area is the same as that of the A320, but it features a Strut-Braced Wing (SBW) [13] with a DHEP configuration. The qualitative trend of the Payload-Range diagrams for the A320 and the INDIGO baseline are shown in Figure 2.

2.2 Mission module

The mission module is split into two main parts. The first part simulates the prescribed mission, which consists of a climb, a cruise segment, a descent, and a diversion consisting of a climb, cruise, and descent at a lower altitude, and a certification 30-minute holding flight. The second part of the module assesses the performance in takeoff and landing for each of the prescribed possible failure cases to find the Takeoff Field Length (TOFL) and Landing Field Length (LFL). Moreover, it calculates climb gradients. For the flight profile of the INDIGO aircraft, a nominal mission range of 1000 NM is selected, with a cruise altitude of $h_{cruise} = 8000$ m and a flight speed of M = 0.6. For the rest of the vertical and horizontal flight speed profiles, radar data corresponding to DH8 aircraft was initially provided by Riga Airport. Given the higher wing loading of the INDIGO aircraft (the same as

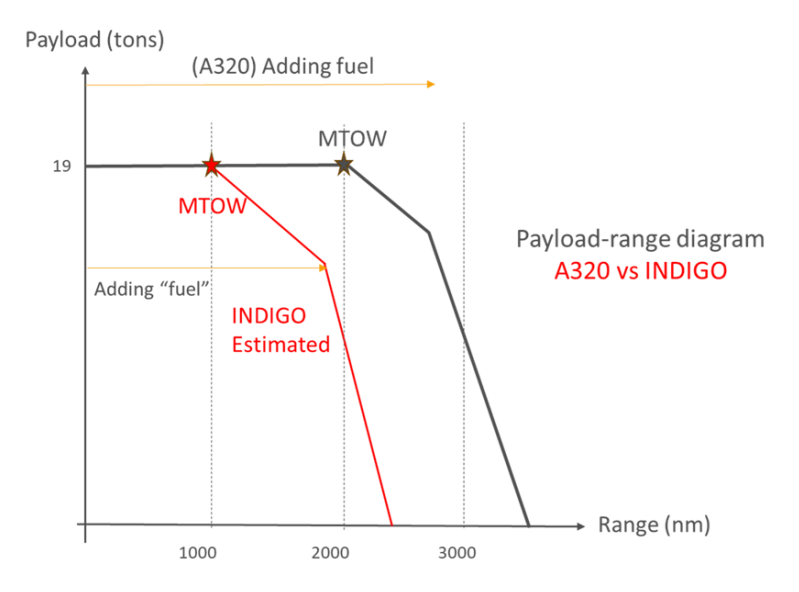


Figure 2 – Estimated Payload-Range diagram for the A320 and INDIGO aircraft.

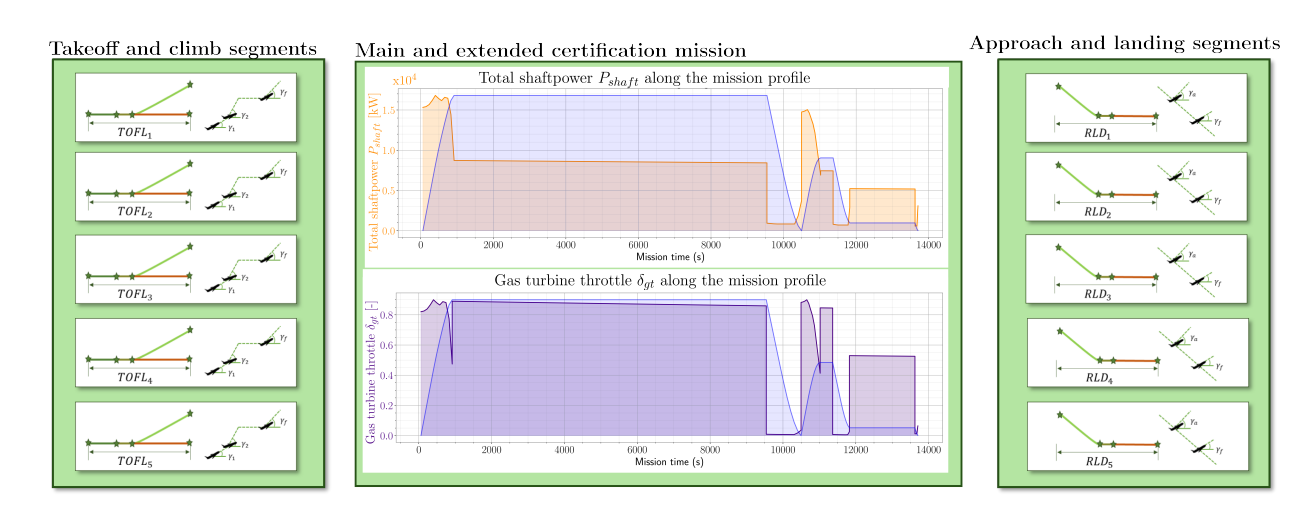


Figure 3 – Description of the mission modularity

the A320), the horizontal speeds at the flight profile low-speed parts were increased to keep the lift coefficient C_L below 1. For the 30 min holding flight, the equivalent airspeed was scaled by $\sqrt{3/4}$ in order to fly near the maximum endurance speed. The altitudes, flight speed, and rate of climb profiles are shown in Figs 4, 5, and 6, respectively.

The maximum takeoff and required landing distances are enforced with constraints at the optimization level. The selected values are similar to those of the A320, with a maximum takeoff length of 2190 m and a maximum landing distance of 1530 m. The climb segments and gradients for both the takeoff and go-around landing segments, according to FAR25 [14], are shown in Table 1 for a twinengine aircraft. These segment angles are enforced as single-point calculations and are applied to evaluate the aircraft feasibility during each failure case scenario. The TOFL, LFL and climb gradients performance deserve a more profound discussion and directive from the certification authorities; the definition of the failure conditions corresponding to the One-Engine-Inoperative of the provided table requires adaptation to DHEP.

In order to calculate the takeoff balanced field length (TOFL), the segments are divided into V_0V_1 , V_1V_R , roll, and V_1V_0 . The segments V_0V_1 and V_1V_R correspond to the phases from zero velocity (V_0) to the decision velocity (V_1) , and from the decision velocity (V_1) to the rotation velocity $(V_R)^1$. The

¹For both the takeoff and landing, the reference speeds are defined according to FAR25 as V_R (1.1 V_{stall}) and V_2 (1.2 V_{stall})

		Take-off	Go-around		
	1° segment	2° segment	3° segment	Approach	Landing
γ_{min}	0%	2.4%	1.2%	2.1%	3.2%
h_{ref}	35 [ft]	400 [ft]	1500 [ft]	-	-
Engine conf.	OEI	OEI	OEI	OEI	AEO
Power set	RTO	RTO	MCT	GA	-
Landing gear	Retraction	Retracted	Retracted	Retracted	Extended
Ref. speed	V_R	V_2	$1.45\ V_{stall}$	-	-
Ref. weight	W. after V_R - V_2	W. after V_R - V_2	Segment end	MLW	MLW
Ground effect	Without	Without	Without	-	-
Flaps conf.	TO	TO	Clean	Approach	Landing

Table 1 – Flight segments and configurations from FAR-25 fro a twin-engine.

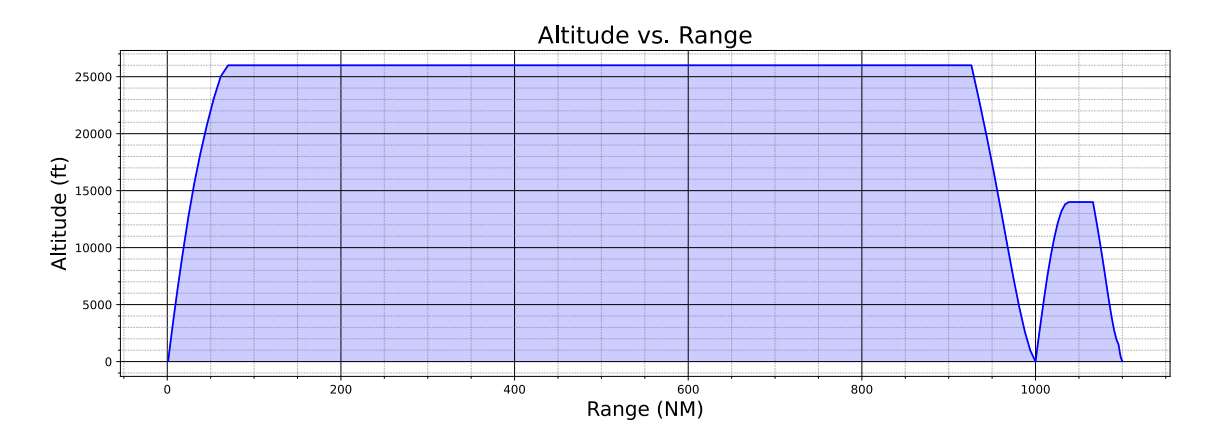


Figure 4 – Altitude profile for the INDIGO reference mission.

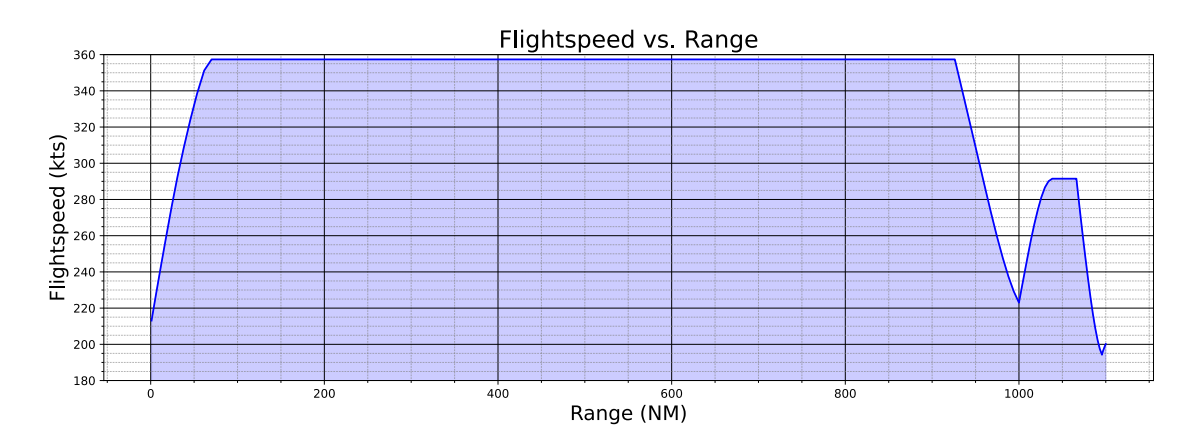


Figure 5 – True airspeed profile for the INDIGO reference mission.

segment V_1V_0 corresponds to the deceleration phase due to a rejected takeoff, going from V_1 to V_0 . The roll segment involves the rolling and initial climb phase from V_R to V_2 , overcoming a reference obstacle. Additionally, a 2-second segment is introduced between V_0V_1 and V_1V_R . A description of the defined segments can be seen in Fig.7. The total distance traveled in each segment is obtained by integrating the following equation of motion:

$$m\frac{dV}{dt} = T - D - \mu(mg - L) \tag{1}$$

Being m the mass of the aircraft, V the velocity, t the time, T and D thrust and drag respectively, and μ the ground friction coefficient (which varies depending on the dry or wet runway). g is the acceleration, and L is the lift.

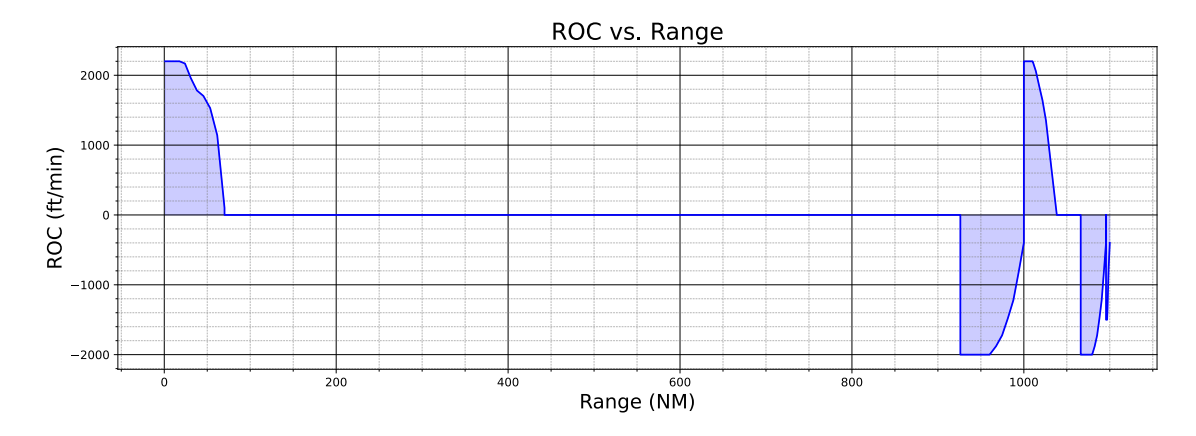


Figure 6 - Rate of climb profile for the INDIGO reference mission.

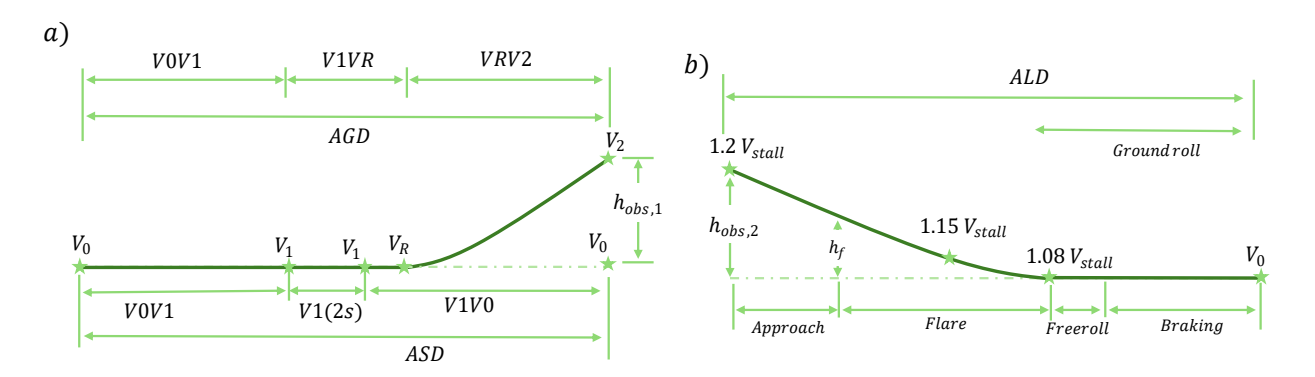


Figure 7 – Takeoff and landing segments for the INDIGO mission.

The required landing distance is obtained via iterative calculation of V_1 through the computation of the Balanced Field Length (BFL). To achieve this, the Accelerate-Go Distance (AGD) must match the Accelerate-Stop Distance (ASD) as shown in Equation (2).

$$BFL \rightarrow AGD = ASD$$
 (2)

The *AGD* is computed as the maximum distance between dry and wet runways considering only the failure case segments, *ASD* is computed as the maximum distance between the dry and wet segments for both All Systems Operatives (ASO, i.e., no failure cases) and the failure cases:

$$ASD = \max\{ASD_{FC,dry}, ASD_{FC,wet}, ASD_{ASO,dry}, ASD_{ASO,wet}\}$$
(3)

$$AGD = \max\{AGD_{FC,drv}, AGD_{FC,wet}\}\tag{4}$$

The TOFL is then computed as the maximum distance between the BFL and 115% of the AGD_{ASO} with all systems operative:

$$AGD_{ASO} = \max\{AGD_{ASO,dry}, AGD_{ASO,wet}\}$$
 (5)

$$TOFL = \max\{1.15 \cdot AGD_{ASO}, BFL\}$$
 (6)

This procedure is repeated independently for each of the failure cases. The landing distance is obtained directly by integrating the segments of approach and flare, the free roll and the braking distance. To comply with the airworthiness regulations this distance is computed with the maximum landing weight (MLW) and a dry landing field surface, for each of the failure cases.

2.3 Powerplant module

For the powertrain a parallel-serial hybrid (PSH) architecture was proposed by the INDIGO consortium research groups at University of Strathclyde, Ruhr University Bochum, Technical University of Braunschweig, and University Carlos III de Madrid. Fig.8 shows a schematic of the PSH architecture implementation. The main quality of the parallel-serial hybrid architecture is the capability of the parallel part to be able to work either by consuming part of the electrical power, or by acting as a partial generator, with fraction of the power being transferred directly to the inboard (IB) propeller shaft, and part of the energy being transferred to the electrical machine coupled to the low pressure turbine shaft.

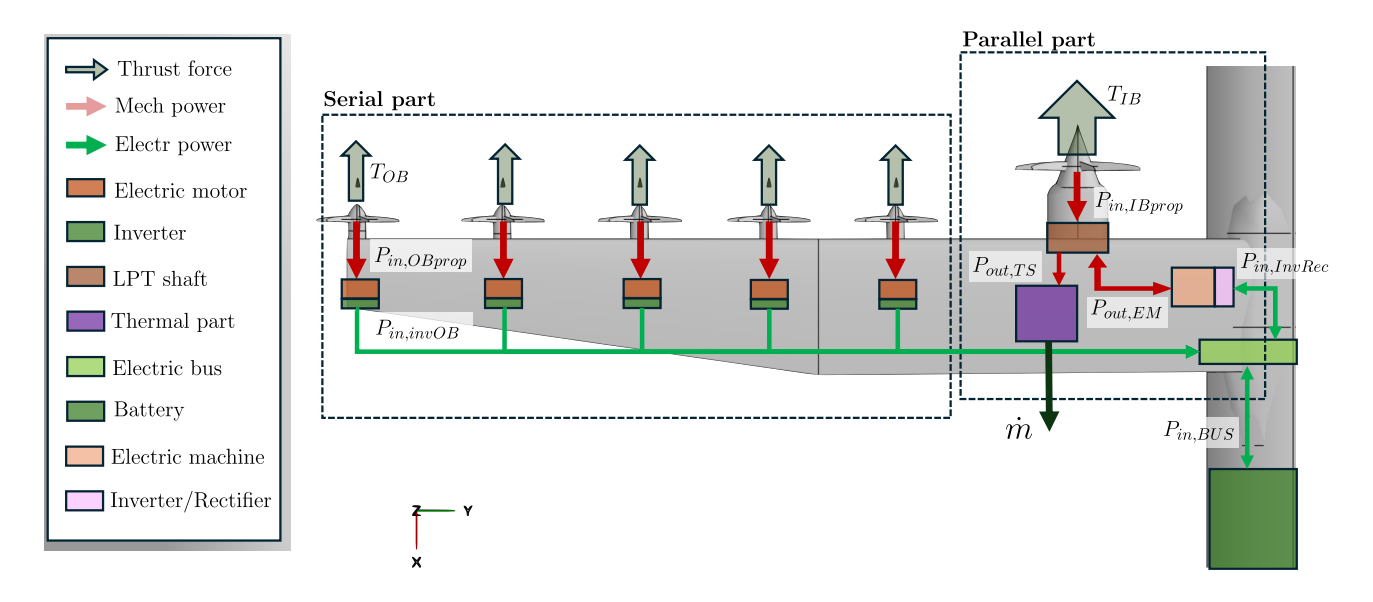


Figure 8 – Description of the parallel-serial hybrid architecture (the direction of the arrows indicate the direction of flow of information, not the flow of power).

The powertrain is simulated by first considering the needed total thrust T to achieve the trim conditions; this thrust is defined as the sum of the thrust given by the inboard and outboard propellers. To control the generated thrust, control state variables δt_{IB} and δt_{OB} are defined; these parameters multiply the maximum output power of the gearbox connected to the low-pressure turbine, and the maximum output power of the OB electric motors, such that the power going into the propellers shafts can be defined as:

$$P_{in,OBprop} = \delta t_{OB} \cdot P_{max,ElectricMotorOB} \tag{7}$$

$$P_{in,IBprop} = \delta t_{IB} \cdot P_{max,GearboxIB} \tag{8}$$

Additionally, to promote an optimal allocation of thrust, the IB and OB throttles are connected by a design variable ψ , that is constant along the flight segment and defines the variable throttle of the propellers:

$$\delta t_{OB} = \psi \cdot \delta t_{IB} \tag{9}$$

Therefore, the produced thrust can be expressed as:

$$T = 2 \cdot n_{prop,OB} \cdot T_{OB}(P_{in,OBprop}, V_{\infty}, \rho) + 2 \cdot T_{IB}(P_{in,OBprop}, V_{\infty}, \rho)$$
(10)

The propeller map defined by the power coefficient C_P and the advance ratio J transforms the input shaft power into thrust. For the low-speed conditions, a propeller static curve of C_T over C_P is used instead. These curves and maps are given in Figure 9. The scaling of these propeller maps has been performed in compliance with established standards [15, 16].

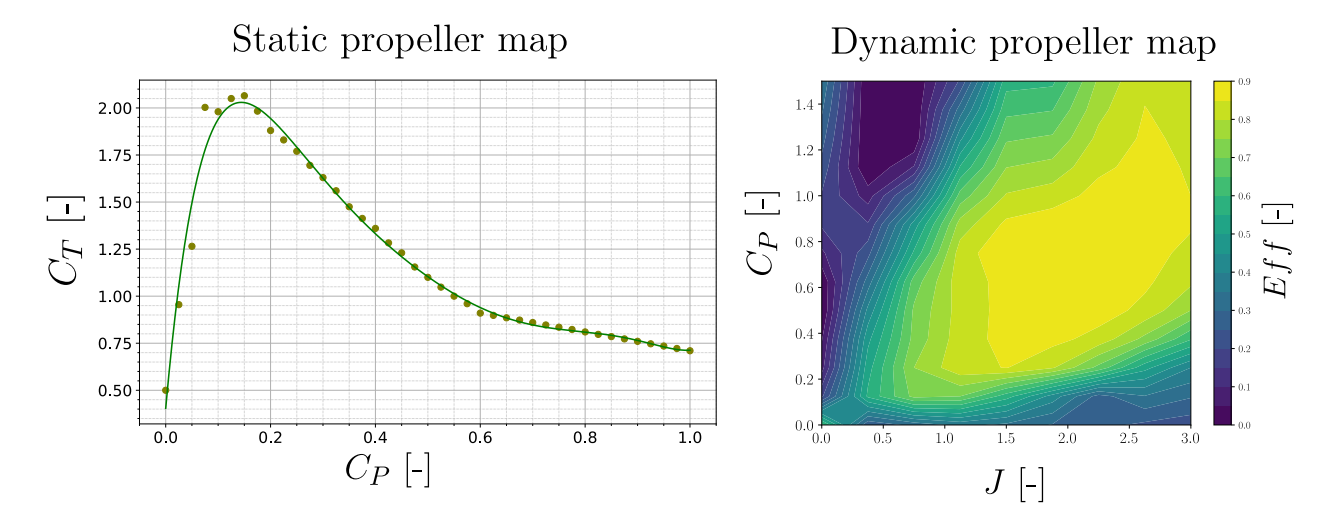


Figure 9 – Static and dynamic propeller maps.

At the same time, the power into the OB propeller shafts goes past the electric motor and through the inverter (with some efficiency losses) and gets summed into the electric bus (the direction is the one of flow of information, not the flow of power). For the case of the parallel part a split of the energy between the IB and the OB has to be performed. To this aim, a local hybridization factor HF^* is defined as:

$$HF^* = \frac{P_{out,EM}}{P_{in,IBprop}} \tag{11}$$

Being $P_{out,EM}$ the amount of power that goes into the electric machine. Given that the electric machine can work as a generator or as an electric motor, positive HF^* indicates that the EM is working as a motor, and negative HF^* values that the EM is working as a generator, with an $HF^*=1$ indicating that the IB propeller shaft is driven only by electric power. Therefore the power that has to be produced by the turbomachinery can be expressed as:

$$P_{out,TS} = P_{in,IBprop} * (1 - HF^*)$$

$$\tag{12}$$

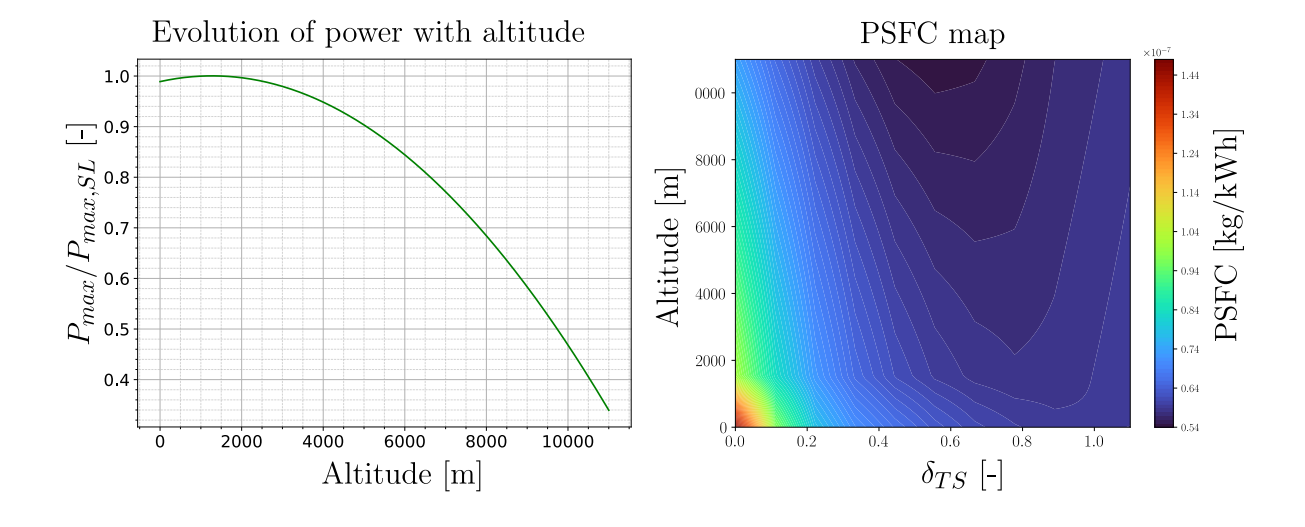


Figure 10 – Power against altitude and PSFC map for the turbomachinery.

The turbomachinery power output is adjusted via a throttle δt_{TS} such that its output shaft power matches the required shaft power from Equation 12. Evolution of the maximum shaft power with

respect to the maximum shaft power at sea level and a map for the PSFC were provided by RUB team (Figure 12) such that the output shaft-power can be defined as Equation 13. The PSFC is employed to compute the fuel flow; this fuel flow is integrated along the given phase to obtain the actual weight of the aircraft.

$$P_{out,TS} = \delta_{TS} \cdot P_{max}(P_{max,SL}, h) \tag{13}$$

The power routed to the electric machine runs through it and through the inverter/rectifier (with some energy losses) until it reaches the electric bus, which distributes power and may recharge the battery.

- If the electric machine (EM) acts as a motor (consuming power), this power is added to the onboard (OB) electric motors' requirements, indicating the system is drawing power.
- If the EM acts as a generator (producing power), this power is subtracted from the OB motors' requirements, potentially recharging the battery if the overall power balance is negative.

The electric bus is modeled to connect both sides of the aircraft and their respective battery packs, allowing any part to consume or supply power to the rest of the system, ensuring efficient energy management and redistribution.

Another relevant parameter to be defined is the global hybridization factor, defined here as the power provided by the battery with respect to the total power:

$$HF = \frac{P_{batt}}{P_{shaft,total}} \tag{14}$$

Notice that this definition can lead to higher than one hybridization factors, as the battery power will always be greater than the electric power into the shaft due to the electrical heat losses.

2.4 Failure cases modeling

The introduction of hybrid architectures increases the complexity of modeling failure cases; while standard aircraft architectures might only suffer the direct loss of an engine as a block (either by a failure in the propeller or a failure in the core of the engine), hybrid architectures can suffer the loss of one of more distributed propulsors or the failure of some of the electrical or thermal components. In this work, these failure cases have been separated into *lack of thrust* (loss of propulsive thrust) or *lack of power* (loss of one source of power production).

2.4.1 Lack of thrust

For scenarios characterized by insufficient thrust, two hypothetical situations are considered: the failure of an inboard propeller along with its nearest outboard counterpart (termed FC1) and the failure of the two outermost tip propellers (referred to as FC2). Given the anticipation that the inboard propeller plays a pivotal role in generating thrust, FC1 is expected to represent a scenario with the most significant reduction in propulsive force. Conversely, the failure of the tip propellers, as outlined in FC2, is assumed to create the most challenging conditions for maintaining control over the yawing moment. These failure cases are depicted in Fig.11. While there is no current airworthiness certification over highly distributed propulsion, this failure case offers a possible worst case of bird strikes with possible blade-off, with the final consequence of having two adjacent propellers inoperative.

2.4.2 Lack of power

For the lack of power models, three hypothetical situations are considered: the loss of a thermal engine (losing the capability of producing power with the turboshaft but still being able to move the shaft with the electric motor) as FC3, losing half of the battery pack (thus reducing the maximum output power from the battery) as FC4, and losing the electric machine part (thus only allowing the IB propeller to be moved by the thermal part) as FC5.

While there is no actual normative for these kinds of hybrid architectures, these failure cases offer a broader view into the possibilities of failure of the power generation systems. Additionally, while the standard takeoff is performed at takeoff throttles ($\delta t_{OB} = 0.9$, $\delta t_{IB} = 0.9$), and lack of thrust FC

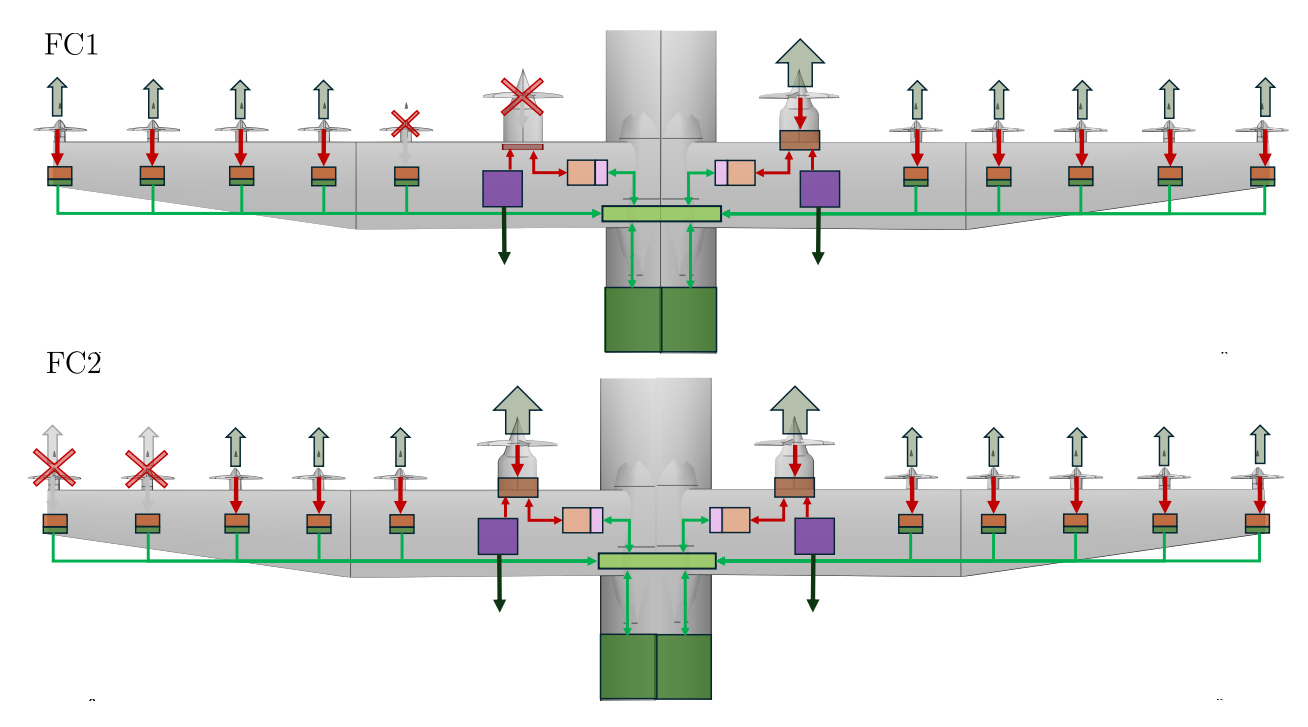


Figure 11 – Description of failure cases FC1 (top) and FC2 (bottom).

are performed at $(\delta t_{OB} = 1, \delta t_{IB} = 1)$, during the lack of thrust failure cases only the inboard thrust is prescribed $(\delta t_{IB} = 0.9)$, leaving the electric part with a higher response rate to reduce part of the thrust to adapt to the maximum total available power.

2.5 Aerodynamic module

For the aerodynamic model the presence of distributed electric propulsion generates a two-way coupling between the thrust and the aerodynamic coefficients. Arranging the equations of horizontal and vertical equilibrium along the wind axes in residual form leads to:

$$\Re_{vert} = W \cdot cos(\gamma) - q \cdot S_{ref} \cdot (CL_{\alpha} \cdot \alpha + CL_0)$$
(15)

$$\Re_{horiz} = T - W \cdot sin(\gamma) - q \cdot S_{ref} \cdot (CD_0 + CD_\alpha \cdot \alpha + CD_{\alpha\alpha} \cdot \alpha^2)$$
(16)

where W represents the weight of the aircraft, γ is the flight path angle, q is the dynamic pressure, S_{ref} is the reference wing surface, α is the angle of attack, and T is the total thrust produced by the propellers. The aerodynamic coefficients CL_0 , CL_α , CD_0 , CD_α , and $CD_{\alpha\alpha}$ are derived from a reduced order model (ROM) [17] created by consortium member UST. This model depends on the propeller disk thrust, flight conditions, and wing platform parameters such as aspect ratio, taper ratio, twist along the wing, strut chord, and strut twist.

For the two-way coupling, the optimizer first takes an initial guess value for the aerodynamic coefficients. With these coefficients, the needed trim thrust is computed by obtaining the needed α from the vertical projection and then obtaining the needed throttle² δt_{IB} to trim the horizontal component; at the same time, the needed power is projected downstream obtaining, for a given local hybridization factor, the needed gas turbine throttle δ_{TS} and therefore the current fuel-flow \dot{m} , to be integrated along the segment to update the aircraft weight.

With this new aircraft mass and propeller thrusts, the aerodynamic coefficients are recomputed, calling once more the ROM and the new value of the state variables δt_{IB} and δ_{TS} . This process is repeated with a Newton method algorithm till the horizontal forces (Equation 16) are balanced. An example of this process is given in Figure 13.

²The OB motor throttle is computed with Equation 9.

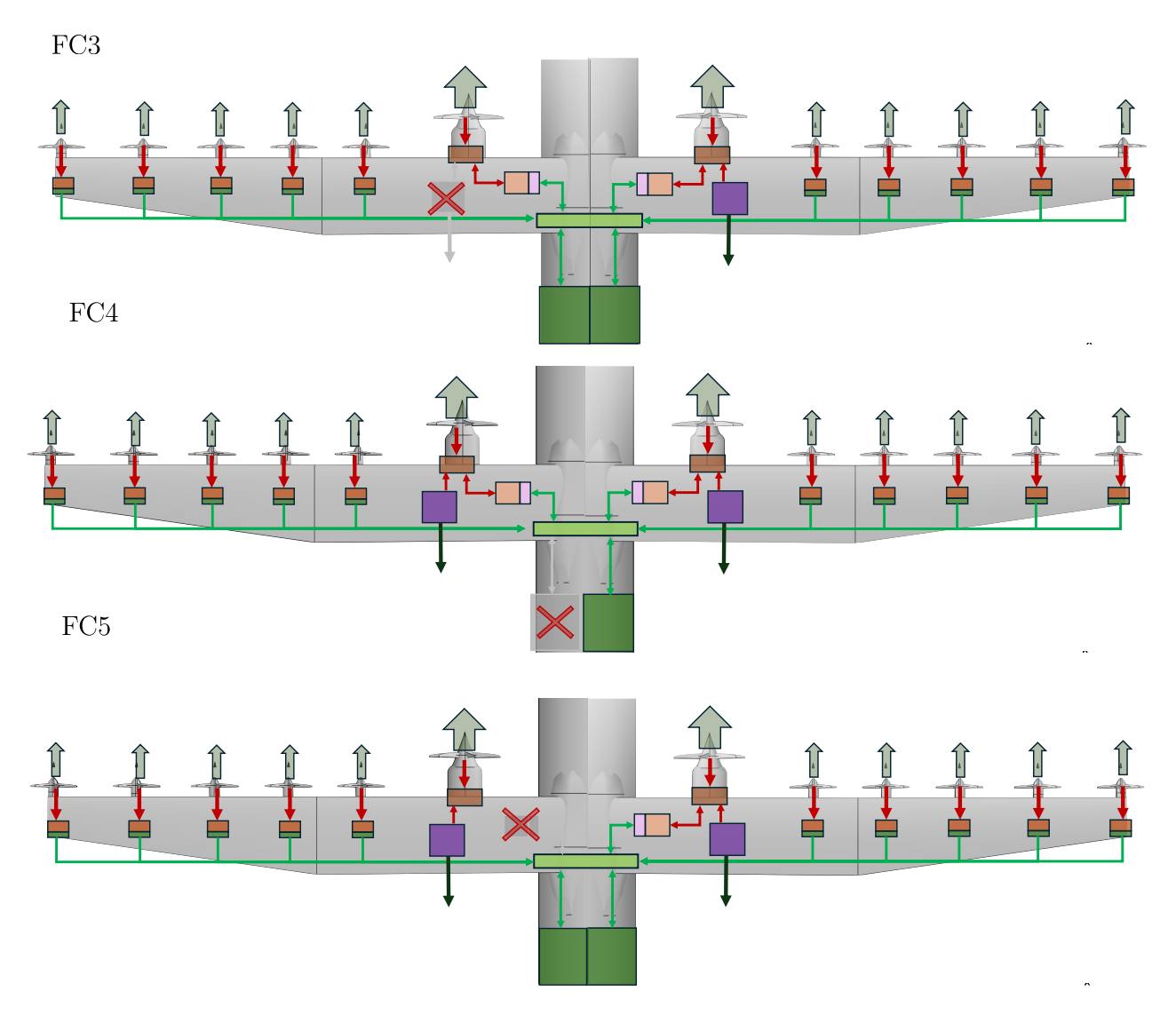


Figure 12 – Description of the FC3 (top), FC4 (middle) and FC5 (bottom).

2.6 Weight module

The weight of the aircraft, obtained from various sources is broken down into operating empty weight OEW, payload weight W_{PL} , fuel weight W_F , and battery weight W_{batt} . At the same time the OEW is subdivided into the structural weight W_{struct} , the system and furnishing weight W_{sys} , $W_{furnishing}$, the weight of the operative items $W_{operitems}$ and the weight of the powerplant system.

$$OEW = W_{struct} + W_{sys} + W_{sys} + W_{furnishing} + W_{operitems}$$
(17)

For the structure, systems, furnishing, and operational items, weights based on various available sources and procedures, from handbook formulas [18, 16, 19, 20] to NASAS's FLOPS [21], were employed. UC3M is currently working on calibrating regression formulas on structural optimization of the wing system and relative fuselage attachments. For the powerplant system, specific weights were provided from a technology roadmap produced by the INDIGO member UST.

In order for the total takeoff TOW weight to not exceed the maximum takeoff weight MTOW, a constraint is imposed over the sum of the battery weight, the OEW, the payload, and the fuel weight.

$$MTOW > TOW = OEW + W_{PL} + W_F + W_{batt}$$
 (18)

This allows the optimizer to trade off the weights of given components (for example, the wing structural weight by varying the aspect ratio AR) against the weight of the batteries and powertrain system.

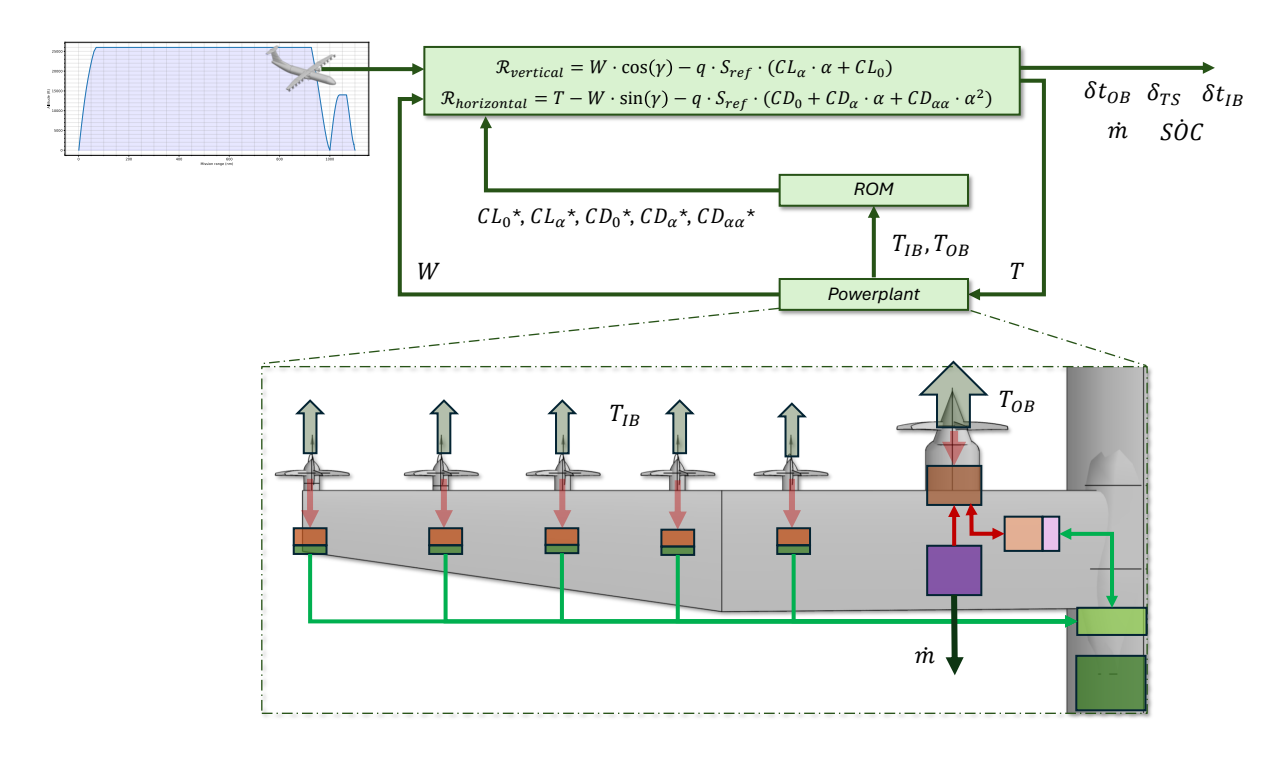


Figure 13 – Iterative process to find the required throttles with two way coupling due to blowing effect.

2.7 Acoustic module

A surrogate model has been developed using Radial Basis functions to analyze the aeroacoustic module and assess the noise generated during takeoff. This model is based on data from the IMMIS+ tool provided by DLR consortium partner. To reduce the number of inputs into the surrogate model, and thus the number of training points, trajectory information such as thrust, shaft power, and speed have been simplified by sampling their values at the start and at the end nodes of each phase. This information acts at the input to the surrogate model. For the training of the surrogate model, the intermediate values, along with the input values, are linearly interpolated, and the *EPN* value is computed according to the ICAO Annex 16 vol 1 [22].

Since IMMIS+ only provides propeller noise data, the primary objective of the aeroacoustic model is not to impose constraints on the emitted noise. Instead, it is intended to be incorporated into the cost function to push the design as much as possible towards an acoustic-friendly solution.

2.8 MDA and MDO

Detailed information on the MDA arrangement, as well as on the MDO strategy can be found in [23], although specialized to a smaller regional aircraft featuring a serial-hybrid or a parallel-hybrid architecture. The authors would like to highlight that the design of the MDA and MDO architectures have been dictated by (i) the need of not restricting the design space, reducing the a-priori decision (ii) the use of a gradient-based optimization, which cannot accept breaks in the MDA. For this paper, the most relevant MDA inputs are:

- i tilis paper, the most relevant MDA inputs are.
- Mission specification: range, cruise altitudes, rate of climb and speeds.
- Geometry parameters: of the fuselage and empennage, and dimensions of the LARW planform.
- Aerodynamic parameters: maximum coefficients of lift during takeoff and landing, $CL_{L_{TO}}^{max}$ and $CL_{L_{IA}}^{max}$, accordingly.
- Operative specifications: MTOW, MLW, maximum pax, max payload, and number of crew members.

- Propulsive specifications: the rating of the power systems, specific weight of the components, battery weight, propeller, and turbo machinery maps and HF* and ψ factors along the mission.
- Mission performance: TOFL, LFL, duration of each phase along the mission, climb angles in certification segments for all FC.
- Weights: OEW and the fuel burnt along the mission W_F .
- Batteries: SOC along the mission profile.

For the design variables, the rating of the components from the powerplant and the design variables that include its operation (HF^* and ψ factors) were included; the design variables for the LARW implemented into the aerodynamic ROM were also included, along the propeller diameter and its tip Mach number. The main constraints for the optimization include all the constraints over the sizing margins of the power-plant components, the certification parameters (TOFL, RFL, and climb gradients), propeller clearance constraints, and SoC of the battery along the mission.

3. Results

3.1 Optimization setup

In the preliminary optimization campaign, the considered battery-specific energy is $Batt_{SE}=400$ Ah/kg, the specific power is $Batt_{SP}=2500$ Wh/kg, and the technological level of the components is aligned with the forecasts for the year 2035 [24, 25]. The State of Charge (SoC) of the battery is constrained not to drop below 20% to avoid early degradation of the performances. The initial cost function has been set to minimize fuel flow throughout the entire mission, and the number of outboard propellers per wing was set to $n_{OB}=3$. It is worth reminding, however, that in INDIGO project the optimization process aims at reducing emissions below 900 m.

The main focus of this paper is the lower bound of the local hybridization factor HF^* . By adjusting this design variable, the degree of serial or parallel operations varies. Lower (negative) HF^* values indicate that the turboshaft is working more as a generator in serial mode, while higher values mean that the turboshaft drives the propeller more like in a parallel architecture. 5 different optimizations have been performed setting the lower bounds to 0, -5, -10, -15, and -20; however, only the latter four produced feasible results.

Each optimization involved 190 design variables (covering component ratings, wing platform variables, propeller variables, and operative variables such as the local hybridization factor HF^* and psi factor ψ) and 620 constraints (encompassing takeoff, landing, and flight gradients, component sizing margins, throttles at the motors and engines, battery state of charge), and took an average of 6.32 hours to run on an R9-5900x machine with 64GB of RAM.

3.2 Optimization results

This section gathers the results of this preliminary optimization campaign and offers a preliminary discussion.

3.2.1 Optimization results

Tab.2 includes some of the results from the optimization along the HF^* lower bound values:

3.2.2 Discussion

Figure 14 shows the selected local hybridization factor at the low-pressure turbine shaft (Equation 16) along the mission profile. As apparent, the optimizer always tries to saturate the maximum hybridization factor during cruise, leaving the turboshaft as a power generator. However Figure 15 suggests that the global hybridization factor (defined in Equation 14) is only slightly affected by the local hybridization factor lower bound variation.

To visualize the role of the battery and the turboshaft, the power generated by the battery and the power out of the low-pressure turbine shaft are shown in Figures 16 and 17, respectively. As apparent, the battery acts like a power booster when the power demand is higher.

Variable	Units	HF* LB -5	HF* LB -10	HF* LB -15	HF* LB -20
Propeller IB diameter	m	3.80	4.01	4.80	3.80
Propeller OB diameter	m	2.33	2.76	2.83	2.36
Propeller IB mach number	None	0.52	0.84	0.84	0.72
Propeller OB mach number	None	0.85	0.85	0.85	0.85
Turboshaft engine rating (SL)	hp	7422.59	7542.44	7254.47	6799.35
Electric motor rating	hp	3815.06	3869.04	3832.90	4018.98
Gearbox rating	hp	1534.12	1358.66	1067.38	532.84
Battery weight	kg	8269.14	9114.98	8796.02	9667.32
Total fuel	kg	6839.72	6788.61	6687.25	6249.42
OEW	kg	43890.63	43095.35	43516.33	43083.24

Table 2 – Sample of results from the optimization cases.

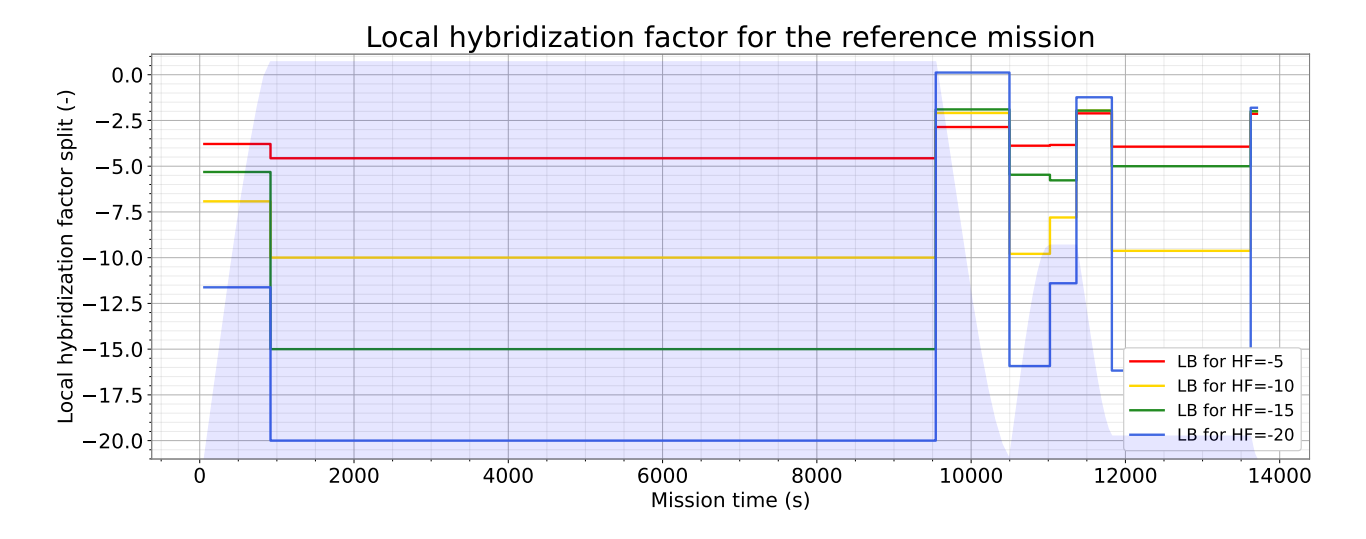


Figure 14 – Local hybridization factor distribution along the mission for different lower HF^* bounds.

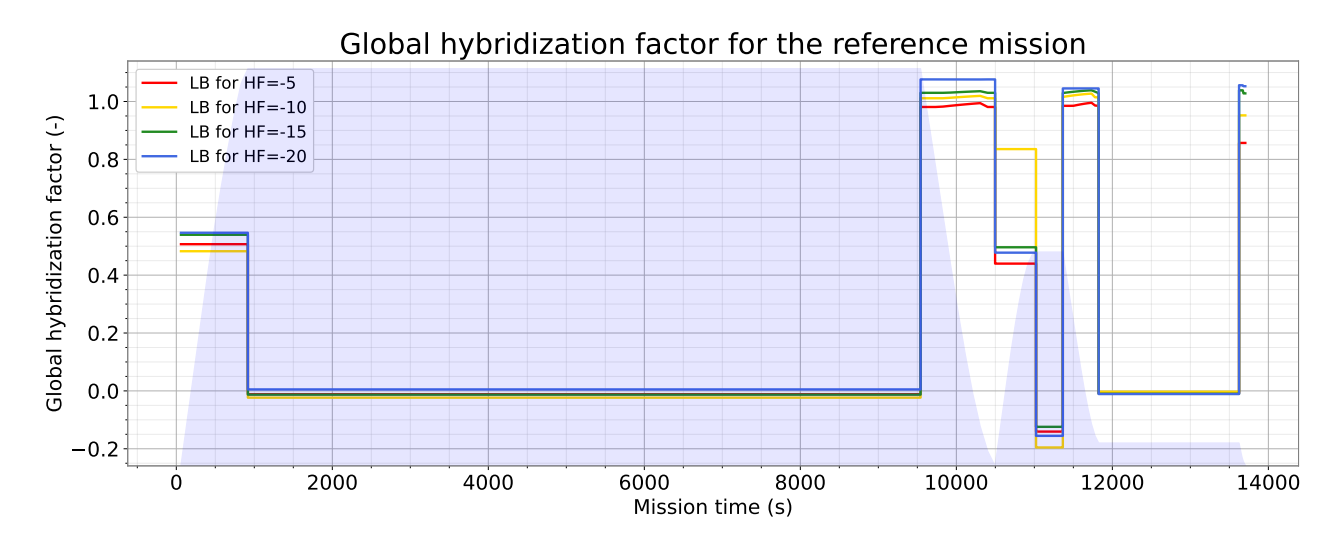


Figure 15 – Global hybridization factor distribution along the mission for different lower HF^* bounds.

Inspecting Figure 18, depicting the the gas turbine throttle distribution along the mission, it can be inferred that the optimizer sizes the gas turbine to operate at its maximum capacity along the climb and cruise segments of the mission. Tracking the state of charge of the battery along the mission profile, Figure 19, it is possible to notice that a slight recharge during the cruise phase occurs, followed by a descend in pure electrical power. It can be speculated that the optimizer prefers to produce the needed electrical power during the cruise phase, where the gas turbine throttle and efficiency are higher. it is worth noticing how the optimizer respects the constraint of having a SoC of the

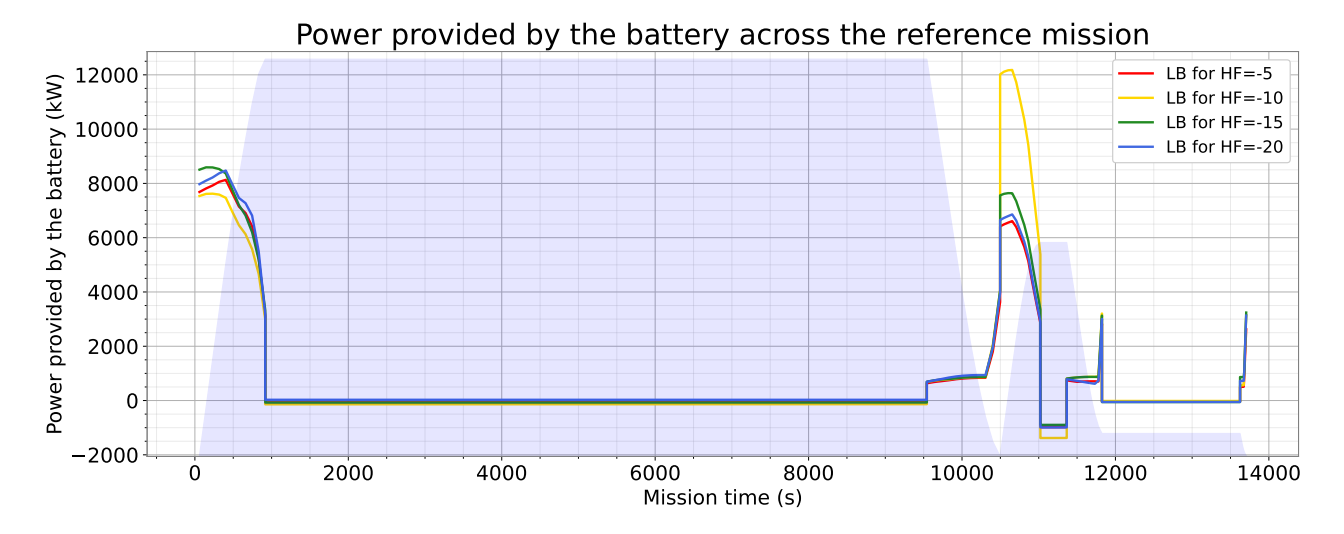


Figure 16 – Power provided by the battery along the mission for different lower HF^* bounds.

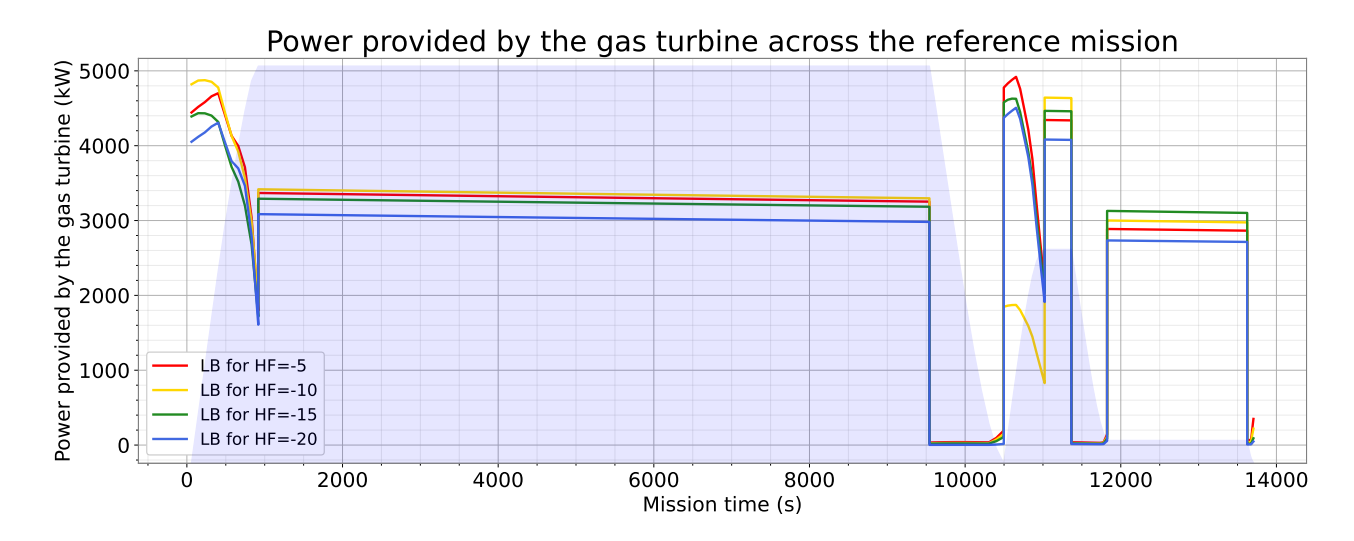


Figure 17 – Power provided by the turboshaft along the mission for different lower HF^* bounds.

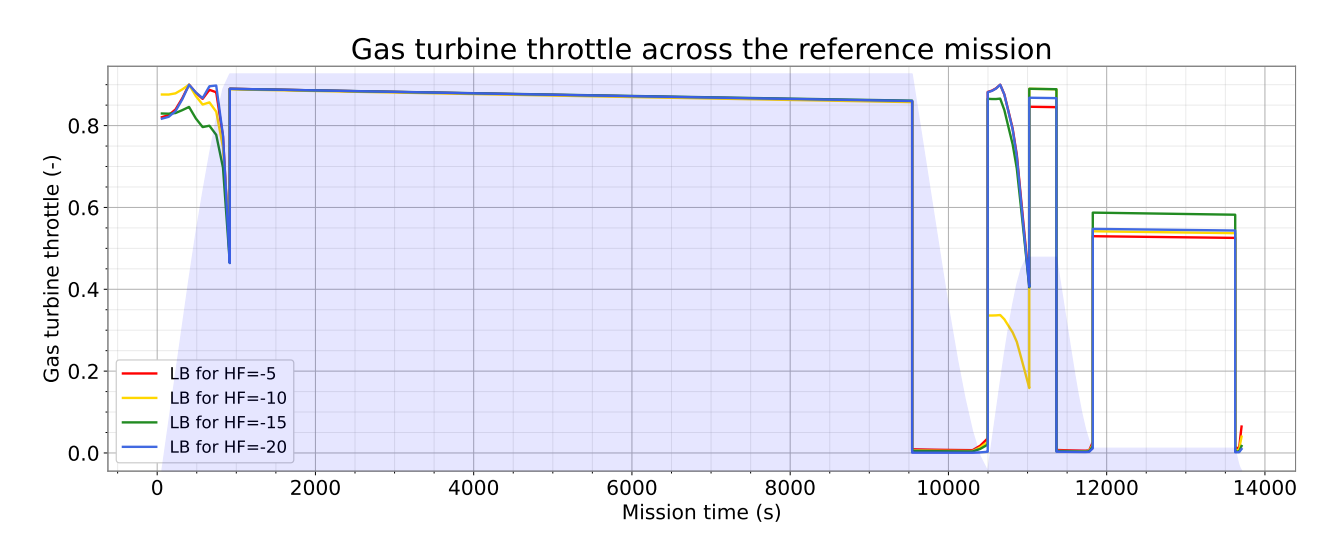


Figure 18 – Throttle of the gas turbine along the mission profile for different lower HF^* bounds.

battery between 20% and 100% along the whole mission. The strategy selected by the optimizer is inherently positive for LAQ leading to aircraft with smaller gas turbine engines always operating

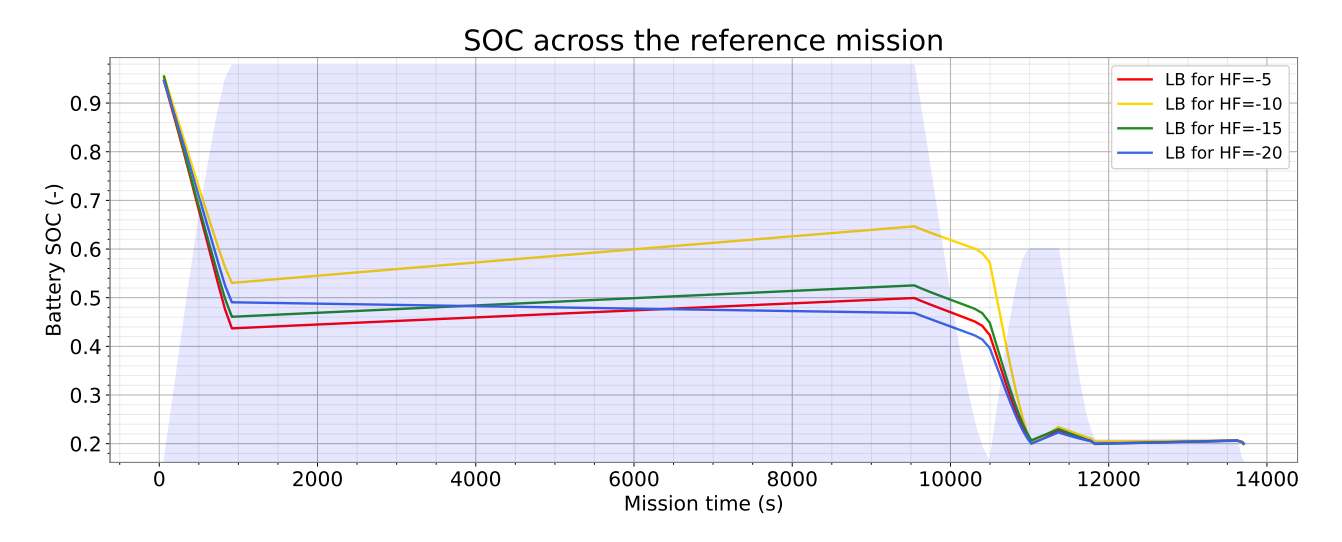


Figure 19 – Battery state of charge along the mission for different lower HF^* bounds.

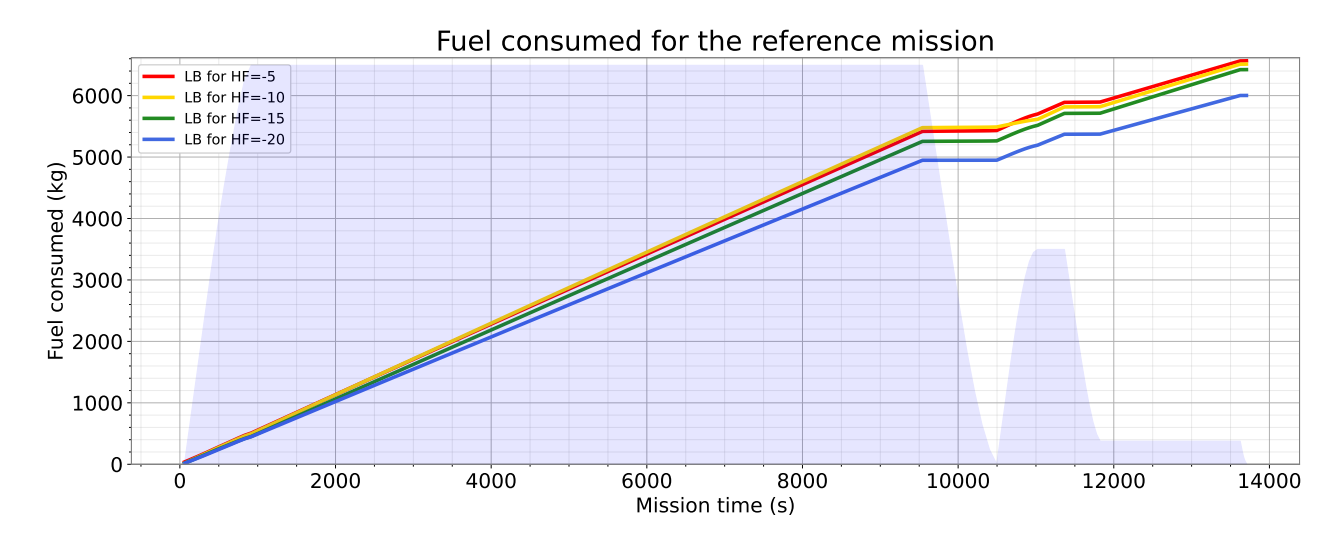


Figure 20 – Fuel burned along the mission for different lower HF^* bounds.

at their maximum continuous performance, with the extra power being provided by the electrical sources. The fuel consumed across the mission is shown in Figure 20.

With respect to the split of the power between the inboard and the outboard propellers, we can see that as the aircraft becomes more serial (lower HF^* values) the thrust provided by the inboard propellers decreases (Figure 21), and so does the efficiency of the inboard propellers (Figure 22). This needs to be further investigated, however, the behavior is most likely driven by the introduction of the FCs into the parallel part during takeoff, rather than seeking for maximum performance of the powertrain when operating in nominal conditions. This stems partially from the operations during FC, where the inboard throttle setting is predetermined; a lower performance rating in the IB propeller reduces the overall electric motor power demand during FC3. In FC3, components that typically function as generators throughout the mission must act as motors, providing all the power to the propeller. However, with a lower propeller rating, less power is needed for it to function as a motor. This evolution can also be seen in Tab.2 where lower bound values for HF^* lead to a reduction in the rating of the IB propeller gearbox assembly.

This preliminary results show the complexity of the MDO problem. Whereas some results can be easily explained, other ones still require a more profound analysis to be fully understood. Such an analysis is of foremost importance to fine-tune the MDO process, refine the overall aircraft modeling, calibrate some discipline models, adjust certain made a priori assumptions (like the FCs), and understand the limiting factors for better performance.

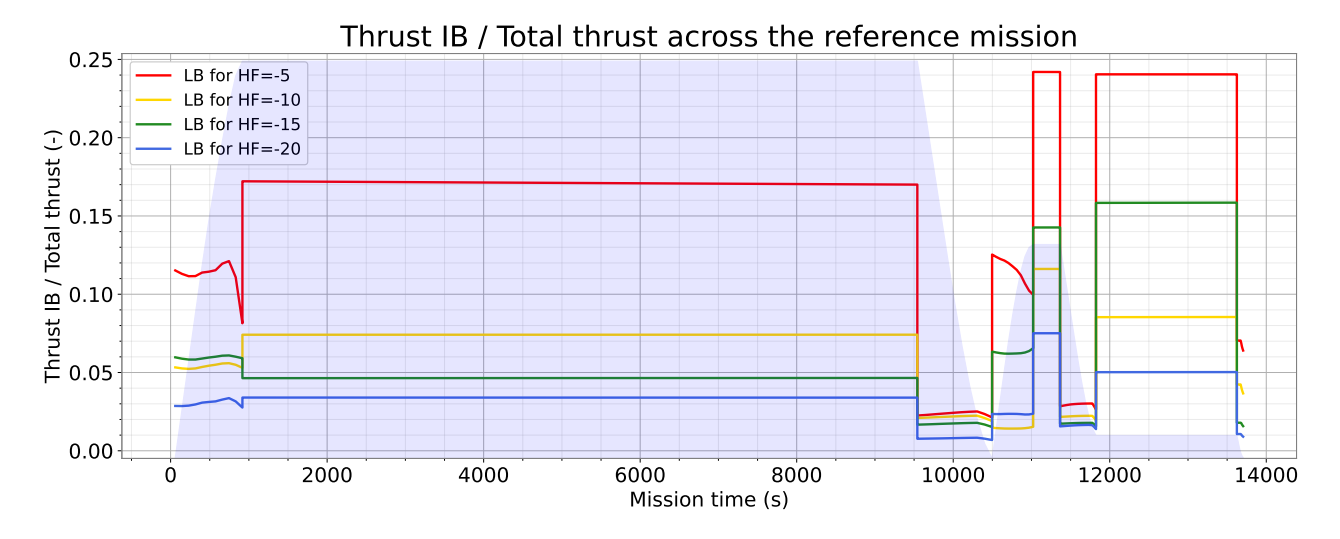


Figure 21 – Ratio of the total thrust generated by the IB propeller with respect to the total thrust across the mission profile and selected lower HF^* bounds.

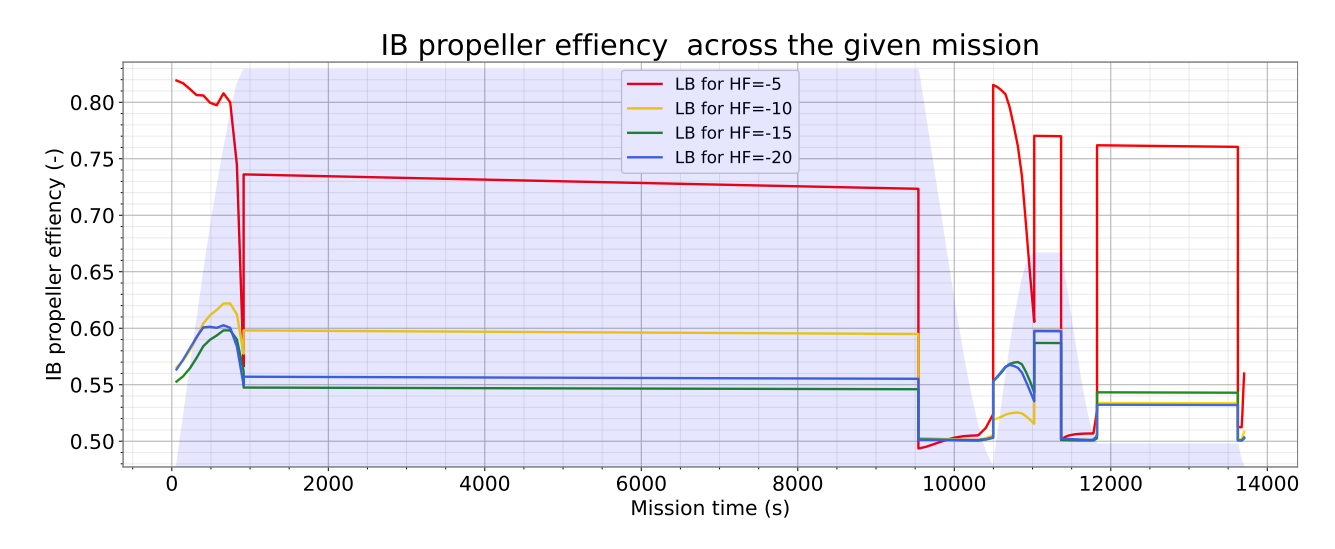


Figure 22 – Efficency of the IB propellers across the mission profile and selected lower HF^* bounds.



Figure 23 – Efficency of the OB propellers across the mission profile and selected lower HF^* bounds.

4. Conclusions

This paper shows the application of a multidisciplinary design optimization procedure to assist the design and optimization of large aspect ratio wings featuring distributed hybrid-electric propulsion technology. Being a novel configuration, classic design procedures and decisions are hardly transferable to the current case, as they are not supported by previous experience. Preliminary results of the optimization campaign show that, to minimize fuel burn, smaller thermal units are selected, operating most of the time at their maximum power, with extra electric power supplied by the batteries when needed. The parallel-serial hybrid architecture functions mostly as a serial configuration, with the thermal part also providing extra energy to power the electric motors driving the outboard propellers. However, the sizing of certain systems is determined by failure case assumptions. For example, it is observed that the outboard propellers generally provide more thrust than the inner ones. The batteries are also recharged in-flight during cruise. Further analysis is currently ongoing to explain in detail the reasons for certain design decisions made by the optimizer.

5. Copyright Statement

The authors confirm that they, and/or their company or organization, hold copyright on all of the original material included in this paper. The authors also confirm that they have obtained permission, from the copyright holder of any third party material included in this paper, to publish it as part of their paper. The authors confirm that they give permission, or have obtained permission from the copyright holder of this paper, for the publication and distribution of this paper as part of the ICAS proceedings or as individual off-prints from the proceedings

6. Acknowledgment

The activities described in this paper have been carried out under the project INDIGO (Integration and Digital Demonstration of Low-emission Aircraft Technologies and Airport Operations), coordinated by Dr. R. Cavallaro from Universidad Carlos III de Madrid. INDIGO project [11] has received funding from the European Climate, Infrastructure and Environment Executive Agency (CINEA) under the Horizon Europe programme under grant agreement No 10109605.

References

- [1] P. Agreement. Paris agreement, 2015. Retrieved December.
- [2] D. S. Lee, G. Pitari, V. Grewe, K. Gierens, J. E. Penner, A. Petzold, M. Prather, U. Schumann, A. Bais, T. Berntsen, et al. Transport impacts on atmosphere and climate: Aviation. *Atmospheric Environment*, 44(37):4678–4734, 2010.
- [3] Karim Abu Salem, Giuseppe Palaia, and Alessandro A. Quarta. Review of hybrid-electric aircraft technologies and designs: Critical analysis and novel solutions. *Progress in Aerospace Sciences*, 141:100924, 2023. Special Issue on Green Aviation.
- [4] Ye XIE, Al SAVVARISAL, Antonios TSOURDOS, Dan ZHANG, and Jason GU. Review of hybrid electric powered aircraft, its conceptual design and energy management methodologies. *Chinese Journal of Aeronautics*, 34(4):432–450, 2021.
- [5] Majid T. Fard, JiangBiao He, Hao Huang, and Yue Cao. Aircraft distributed electric propulsion technologies—a review. *IEEE Transactions on Transportation Electrification*, 8(4):4067–4090, 2022.
- [6] Hyun D. Kim, Aaron T. Perry, and Phillip J. Ansell. A review of distributed electric propulsion concepts for air vehicle technology. In *2018 AIAA/IEEE Electric Aircraft Technologies Symposium (EATS)*, pages 1–21, 2018.
- [7] Jaroslaw Sobieszczanski-Sobieski, Alan Morris, Michel J.L. van Tooren, Gianfranco La Rocca, and Wen Yao. *Multidisciplinary Design Optimization Supported by Knowledge Based Engineering*. John Wiley & Sons, Ltd., 8 2015.
- [8] Joaquim R. R. A. Martins and Andrew Ning. *Engineering Design Optimization*. Cambridge University Press, Jan 2022.
- [9] Benjamin J Brelje and Joaquim RRA Martins. Development of a conceptual design model for aircraft electric propulsion with efficient gradients. In 2018 AIAA/IEEE electric aircraft technologies symposium (EATS), pages 1–25. IEEE, 2018.

LAQN Optimization of a Large Aspect-Ratio Wings with Distributed Hybrid Electric Propulsion

- [10] Raúl Quibén Figueroa, Rauno Cavallaro, Andrea Cini, and Manuel Soler Arnedo. Motivation (mdao for sustainable aviation)-framework development for the design and optimization of h2 powered aircraft. In *AIAA AVIATION 2023 Forum*, page 4151, 2023.
- [11] Innovative aircraft and propulsion technologies to improve air quality near airports.
- [12] Justin S Gray, John T Hwang, Joaquim RRA Martins, Kenneth T Moore, and Bret A Naylor. Openm-dao: An open-source framework for multidisciplinary design, analysis, and optimization. *Structural and Multidisciplinary Optimization*, 59(4):1075–1104, 2019.
- [13] Rauno Cavallaro and Luciano Demasi. Challenges, ideas, and innovations of joined-wing configurations: A concept from the past, an opportunity for the future. *Progress in Aerospace Sciences*, 87:1–93, 2016.
- [14] EASA. Far/cs25 aircraft regulation. Federal Aviation Administration, 2021.
- [15] Standard Hamilton. Generalized method of propeller performance estimation 1961-1963, 1963.
- [16] A.K. Kundu, M.A. Price, and D. Riordan. *Conceptual Aircraft Design: An Industrial Approach*. John Wiley & Sons, Hoboken, USA, 1st edition, 2019.
- [17] Marco Fossati, Bryn Jones, Peter Nagy, and Edmondo Minisci. *An aerodynamic parametric study of large aspect-ratio wings with distributed propulsion for conceptual airframe definition.*
- [18] Mahmoud Fouda, Eytan J. Adler, Jasper H. Bussemaker, Joaquim R.R.A. Martins, D.F, Kurtulus, and Luca Boggero Björn Nagel. Automated hybrid propulsion model construction forconceptual aircraft design and optimization, 2022.
- [19] Jan Roskam. Airplane Design Part I through VIII. DARcorporation, Lawrence, Kansas, 5 edition, 2018.
- [20] Denis Howe. *Aircraft Conceptual Design Synthesis*. Professional Engineering Publishing Limited, London and Bury St Edmunds, UK, 1 edition, 2000.
- [21] Douglas P. Wells, Bryce L. Horvath, and Linwood A. McCullers. The flight optimization system: Weights estimation method. NASA Technical Memorandum TM–2017–219627/Volume I, Langley Research Center, Hampton, Virginia and ATK Space Systems, Inc., Hampton, Virginia, Hampton, Virginia 23681-2199, 2017.
- [22] International Civil Aviation Organization (ICAO). *Annex 16 Environmental Protection Volume I Aircraft Noise*. ICAO, 8th edition, 7 2017. Includes Amendments no. 13 and 14.
- [23] Raul Quiben Figueroa, Rauno Cavallaro, and Andrea Cini. Feasibility studies on regional aircraft retrofitted with hybrid-electric powertrains. *Aerospace Science and Technology*, 151:109246, 2024.
- [24] Reynard de Vries, Malcom Brown, and Roelof Vos. Preliminary sizing method for hybrid-electric distributed-propulsion aircraft. *Journal of Aircraft*, 56(6):2172–2188, nov 2019.
- [25] Benjamin J Brelje and Joaquim RRA Martins. Electric, hybrid, and turboelectric fixed-wing aircraft: A review of concepts, models, and design approaches. *Progress in Aerospace Sciences*, 104:1–19, 2019.